Biochimica et Biophysica Acta 1828 (2013) 1953–1961

Contents lists available at SciVerse ScienceDirect

Biochimica et Biophysica Acta

journal homepage: www.elsevier.com/locate/bbamem

Huntingtin disrupts lipid bilayers in a polyQ-length dependent manner

Kathleen A. Burke [a], Kaitlin M. Hensal [a], C. Samuel Umbaugh [a], Maxmore Chaibva [a,b], Justin Legleiter [a,b,c,*]

[a] The C. Eugene Bennett Department of Chemistry, West Virginia University, Morgantown, WV 26505, USA
[b] NanoSAFE, West Virginia University, Morgantown, WV 26505, USA
[c] The Center for Neurosciences, West Virginia University, Morgantown, WV 26505, USA

ARTICLE INFO

Article history:
Received 26 November 2012
Received in revised form 25 April 2013
Accepted 26 April 2013
Available online 2 May 2013

Keywords:
Polyglutamine
Huntingtin
Huntington's disease
Atomic force microscopy
Protein aggregation
Supported lipid bilayer

ABSTRACT

Huntington's Disease (HD) is a neurodegenerative disorder that is defined by the accumulation of nanoscale aggregates comprised of the huntingtin (htt) protein. Aggregation is directly caused by an expanded polyglutamine (polyQ) domain in htt, leading to a diverse population of aggregate species, such as oligomers, fibrils, and annular aggregates. Furthermore, the length of this polyQ domain is directly related to onset and severity of disease. The first 17 N-terminal amino acids of htt have been shown to further modulate aggregation. Additionally, these 17 amino acids appear to have lipid binding properties as htt interacts with a variety of membrane-containing structures present in cells, such as organelles, and interactions with these membrane surfaces may further modulate htt aggregation. To investigate the interaction between htt exon1 and lipid bilayers, in situ atomic force microscopy (AFM) was used to directly monitor the aggregation of htt exon1 constructs with varying Q-lengths (35Q, 46Q, 51Q, and myc-53Q) on supported lipid membranes comprised of total brain lipid extract. The exon1 fragments accumulated on the lipid membranes, causing disruption of the membrane, in a polyQ dependent manner. Furthermore, the addition of an N-terminal myc-tag to the htt exon1 fragments impeded the interaction of htt with the bilayer.

1. Introduction

Huntington's disease (HD), a fatal neurodegenerative disorder, is caused by a CAG repeat encoding a polyglutamine (polyQ) expansion within the first exon of huntingtin (htt) [1]. There are ten known expanded CAG repeat diseases in which polyQ expansion beyond a specific threshold length results in progressive neurodegeneration [2]. In HD, the expanded polyQ domain is responsible for the formation and deposition of intranuclear and cytoplasmic inclusion bodies composed of fibrillar htt aggregates in transgenic mouse models and HD brain tissues [3–5].

An important hallmark of HD is that age-of-onset and disease severity are correlated with the length of the polyQ stretch. PolyQ repeats smaller than 35 are not associated with disease, 36–39 repeats result in reduced penetrance, 40–59 repeats result in adult age-of-onset, and greater than 60 repeats yield juvenile forms of HD [6–8]. As mutant htt fragments containing at least 39Q form detergent-insoluble protein aggregates characteristic of amyloid fibrils in a polyQ length dependent manner [9,10], it was hypothesized that htt aggregation initiated by expanded polyQ is associated with toxicity in HD. Furthermore, a series of AFM studies demonstrated that htt aggregates into a variety of oligomers and fibrils in a polyQ length and concentration dependent manner [11]. Interestingly, synthetic polyQ peptides are capable of forming fibrils with polyQ domain lengths well below the disease threshold [11,12]. The aggregation pathway and rate of aggregate formation of these synthetic polyQ peptides are altered by the addition of flanking sequences associated with htt [13,14].

Upon the discovery that behavioral phenotype followed the appearance of intranuclear and cytoplasmic inclusion bodies in mouse models, it was hypothesized that the formation of inclusions was directly involved in HD pathology [3]. Mutant htt fragments in cell culture formed cytoplasmic and intranuclear inclusions in a polyQ dependent manner [15–17]. However, the role of inclusions in HD was challenged by studies demonstrating that inclusions might be protective or incidental while the smaller more diffuse population of aggregates may represent toxic entities [16,18,19]. Crystallographic and antibody studies have highlighted the diversity of htt exon1 conformers [20,21], demonstrating the complexity of potential aggregation starting points driven by polyQ expansion.

Several potential functions of htt have been postulated, providing insight into possible modes of toxicity. Htt has been shown to aid in orienting mitotic spindles during cell division [22], transporting vesicles along microtubules [23], and associating with the endoplasmic reticulum [24,25] and nucleus [26]. The first 17 N-terminal amino acids (Nt17) in htt exon1 have been shown to adopt a highly conserved amphipathic α-helical structure with membrane binding properties [24], pointing to the potential importance of htt exon1's interaction with lipid membranes. The interaction and insertion of htt with plasma membranes have been shown to be polyQ dependent [27–29]. Thus, the availability of Nt17 as well as polyQ length appears

* Corresponding author at: Department of Chemistry, West Virginia University, USA. Tel.: +1 304 293 0175; fax: +1 304 293 4904.
E-mail address: justin.legleiter@mail.wvu.edu (J. Legleiter).

0005-2736/$ – see front matter © 2013 Elsevier B.V. All rights reserved.
http://dx.doi.org/10.1016/j.bbamem.2013.04.025

to modulate htt exon1/lipid interaction. A recent study involving the intraventricular infusion of ganglioside GM1 induced phosphorylation of residues 13 and 16 within the 17 N-terminal amino acids and attenuated htt toxicity and restored normal motor function [30].

As polyQ length modulates aggregation state, membrane association, and onset and severity of disease, the extent of association and morphology of toxic conformers at lipid interfaces may also be polyQ length dependent. Here, we sought to systematically quantify the role of polyQ length in htt exon1 aggregation at lipid membrane interfaces and determine the impact of this aggregation on membrane mechanical properties. We also investigate the role of Nt17 in facilitating htt/lipid bilayer interaction. Due to the limitations of traditional light and electron microscopy approaches for studying heterogeneous mixtures of htt aggregates on biological surfaces, we used atomic force microscopy (AFM) to characterize the morphology and roughness of the supported model membranes. AFM yields three-dimensional surface maps with nanometer resolution in solution with the absence of artifacts from sample processing. By using a specialized variation of in situ tapping mode AFM called scanning probe acceleration microscopy (SPAM), mechanical surface properties, such as compression and adhesion, can be measured locally. Furthermore, both techniques are operable in aqueous environments, making them uniquely well suited for biologically relevant samples.

2. Materials and methods

2.1. Purification of GST-htt-exon1 fusion proteins

Glutathione S-transferase (GST)-Htt exon1 fusion proteins were purified as previously described [31]. For experiments presented here, four different htt exon1 fragments were used (Fig. 1a): (1) htt exon1(35Q), which contains 35 repeat glutamines, (2) htt exon1(46Q), which contains 46 repeat glutamines, (3) htt exon1(51Q), which contains 51 repeat glutamines, and (4) myc-htt exon1(53Q), which contains 53 repeat glutamines and an additional N-terminal myc-tag that is not present in the other constructs. Briefly, the GST-htt fusion proteins were expressed by induction in *Escherichia coli* with isopropyl β-D-thiogalactoside at 30 °C for 4 h. Lysozyme (0.5 mg/mL) was used to lyse the cells. The fusion proteins were purified from lysate by using a GST affinity column and liquid chromatography (LPLC, BioRad or FPLC, GE Pharmacia). Relevant fraction and purity was determined by gel electrophoresis (Fig. 1b). Purity of the fusion proteins was consistently greater than 90% for all polyQ lengths based on Coomassie blue staining. Cleavage of the GST moiety by PreScission Protease (GE Healthcare, Piscataway, NJ) or Factor Xa (Promega, Madison, WI) initiates aggregation (Fig. 1c). Fresh GST-htt exon1 fusion proteins were used for each experiment. Solutions with all fusion proteins were centrifuged at 20,000 ×*g* for 30 min at 4 °C to remove preexisting aggregates prior to the addition of the cleaving agent, and all experiments were carried out in buffer A (50 mM Tris–HCl, pH 7.0, 150 mM NaCl, 1 mM DTT). To ensure efficient GST cleavage, the GST-htt exon1 fusion protein and respective cleavage agents were incubated for 1 h on ice.

2.2. Preparation of defect free bilayers patches

Lyophilized total brain lipid extract (porcine) was purchased from Avanti Polar Lipids (Alabaster, AL) and resuspended in phosphate buffered saline (PBS) (pH 7.3) at a concentration of 1 mg/mL. By using a liquid nitrogen ice bath, bilayers and multilayer lipid sheets were formed by five cycles of freeze–thaw treatment. Vesicle formation within the lipid suspensions was promoted by bath sonication for 30 min. All experiments were performed with the same lot of lipids. 25 μL of the suspended vesicle solution, diluted with 25 μL of PBS (pH 7.3), was added directly to the AFM fluid cell and placed onto freshly cleaved mica. Vesicles were allowed to absorb to the mica and fuse together to form a defect free bilayer (40 × 40 μm). Once the bilayer formed, 2–3 washes with PBS were performed to remove excess lipid vesicles.

2.3. In situ AFM imaging conditions

In situ AFM experiments were performed with a Nanoscope V MultiMode scanning probe microscope (Veeco, Santa Barbara, CA) equipped with a sealable fluid cell and a closed-loop vertical engage J-scanner. Images were taken with V-shaped oxide-sharpened silicon nitride cantilever with a nominal spring constant of 0.5 N/m (Veeco, Santa Barbara, CA) or with diving board shaped silicon cantilevers with a nominal spring constant of 0.1 N/m (VISTAprobes, Phoenix, AZ). Scan rates were set at 1.95 Hz with cantilever drive frequencies ranging from 7 to 9 kHz. Proteins were prepared as previously described to a final concentration of 20 μM in PBS at a pH 7–8 when injected directly into a fluid cell containing a defect-free bilayer. The bilayer surface was continually imaged once the protein was injected.

For SPAM experiments, 5 × 1.25 μm tapping mode AFM images were captured with 512 × 128 pixel resolution. A signal access module (Veeco, Santa Barbara, CA) and CompuScope 14100 data acquisition card (Gage, Lachine, Quebec) were used to capture the cantilever deflection signal at 2.5 MS/s and 14-bit resolution with a vertical range of 2 V. The cantilever deflection signals were filtered with a sliding, Fourier transform based harmonic comb filter, and the second derivative of the filtered cantilever deflection signal was used to acquire tip acceleration. Tip acceleration was multiplied by the effective cantilever mass, m_{eff}, resulting in the recovery of the time-resolved tapping force between the tip and sample [32]. The m_{eff} was obtained via thermal cantilever calibration methods [33].

2.4. Image processing

AFM images were analyzed with Matlab equipped with the image processing toolbox (Mathworks, Natick, MA). Physical dimensions of aggregates were measured automatically in the following way [34,35]: (1) Images were imported into Matlab. (2) A flattening algorithm was applied to correct for curvature due to the imaging process. (3) Binary maps of aggregate location were created from the flattened images by using a height threshold. This was accomplished by assigning values of 0 or 1 to any pixel of the image that represented a height below or above the allocated threshold, respectively. (4) Discrete aggregates were located by applying pattern recognition algorithms to the binary map. (5) Once a discrete aggregate was located, physical properties were measured automatically. Each aggregate was also assigned an individual number so that aggregates chosen based on specific measured properties could be located, allowing us to verify that chosen dimensions correspondent to specific aggregate types.

3. Results

3.1. Htt exon1 interacts with lipid bilayers in a polyQ length dependent

To determine the extent that htt exon1 interacts with lipid bilayers, we prepared supported, model lipid membranes through fusion of total brain lipid extract (TBLE) vesicles. The formation of supported lipid bilayers by vesicle fusion is well established [36–38], and such bilayers preserve many of the properties (i.e., lateral fluidity) of their free membrane counterparts [36,37]. Moreover, TBLE bilayers represent an appropriate model surface for studies aimed at elucidating the interaction of htt with lipids as TBLE is comprised of a physiologically relevant ratio of membrane components, i.e., acidic and neutral phospholipids, gangliosides, cholesterol, sphingolipids, and isoprenoids. All experiments were performed at 21–22 °C.

Defect free bilayers (as determined by AFM) were exposed to htt exon1 proteins with various polyQ lengths (htt exon1(35Q), htt exon1(46Q), and htt exon1(51Q)) that were purified from *E. coli*

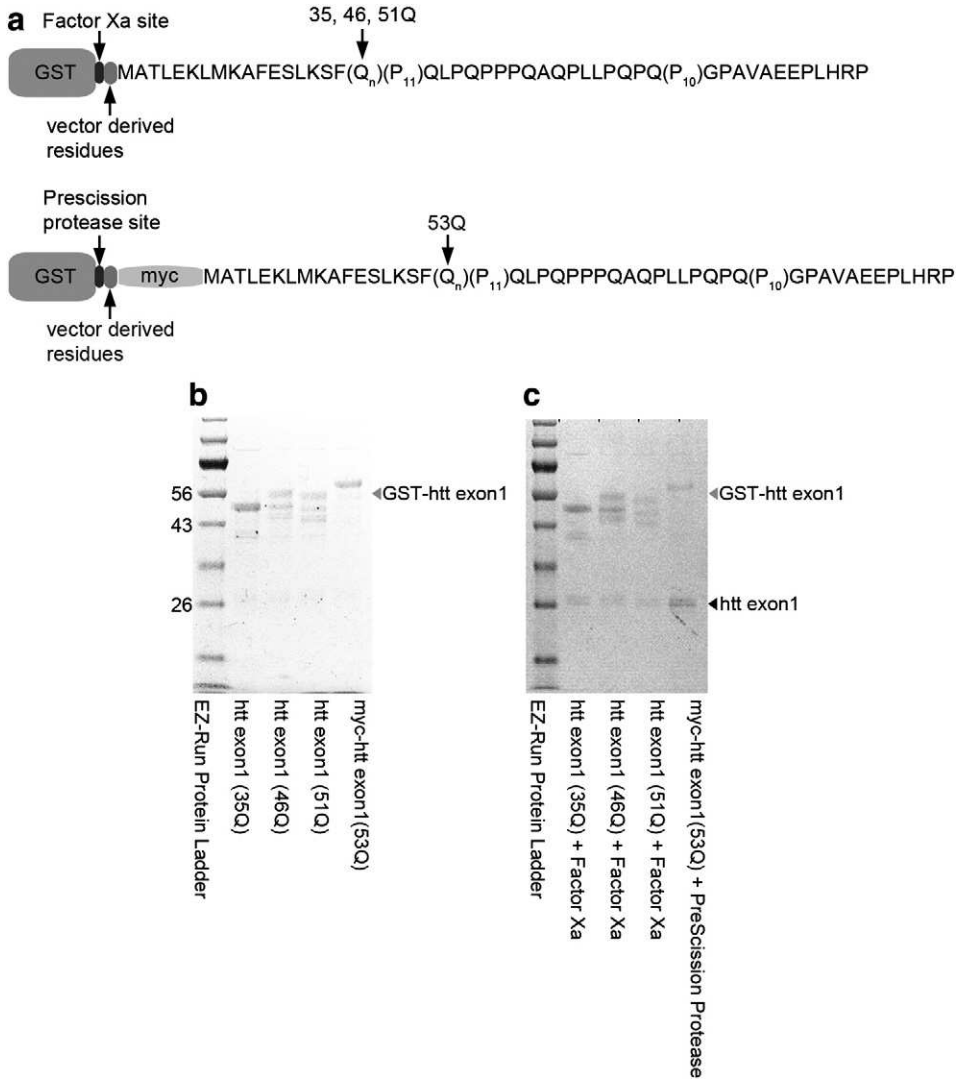

Fig. 1. (a) Schematic representations (not to scale) of the GST-htt exon1 fusion proteins (htt exon1(35Q), (46Q), (51Q), and myc-htt exon1(53Q)) used in this study. The fusion proteins contain a GST tag, which upon addition of Factor Xa or PreScission Protease, cleaves this tag and initiates aggregation. (b) Representative SDS-PAGE of the purified fusion proteins demonstrating the relative purity of each sample. (c) SDS-PAGE demonstrating the efficiency of cleaving the GST tag of the different fusion proteins.

as a glutathione S-transferase (GST) fusion protein. To cleave the GST moiety and initiate aggregation, Factor Xa was incubated with the GST-exon1 fusion protein on ice for 1 h prior to exposure to the supported bilayer. At such a time point, the resulting htt exon1 preparations predominately contain monomers and small oligomers [11,34]. Exposure of the membrane to vehicle buffers containing no htt protein did not result in any changes in the bilayer morphology after the initial injection and for at least 15 h after injection (Fig. 2a).

Upon the initial exposure of the TBLE bilayer to 20 μM freshly prepared htt exon1(35Q), there was noticeable deposition of protein aggregates on the bilayer. Within 1–3 h of exposure (Fig. 2b), there were both regions of perturbed bilayer morphology (evidenced by an increase in RMS surface roughness) and discrete, amorphous aggregates of htt exon1(35Q) on or potentially in the bilayer. These aggregates were stable and immobile on the bilayer surface. There were also small numbers of oligomers, based on morphology, observed on the surface. In successive images, these amorphous aggregates became larger, increasing in volume. The extent of bilayer perturbed by htt exon1(35Q) also increased with time. After 12 h (Fig. 2b) of exposure to htt exon1(35Q), the extent of bilayer disruption increased in area, indicating further disruption of the bilayer's structural integrity.

When TBLE bilayers were exposed 20 μM aliquots of htt exon1(46Q), large, discrete patches of roughened bilayer also appeared within 1–4 h (Fig. 2c) with a similar morphology, stability, and immobility as was observed for htt exon1(35Q) on the lipid bilayer. The extent of bilayer disruption caused by htt exon1(46Q) increased with time. After ~12 h (Fig. 2c) of exposure of htt exon1(46Q), a vast area of bilayer roughness was observed. Htt exon1(46Q) aggregates also formed on the bilayer surface. While there were discrete oligomers observed, large amorphous accumulations of htt exon1(46Q) that grew in mass with time were also present.

When TBLE bilayers were exposed to 20 μM solutions of htt exon1(51Q), extensive areas of the bilayer were disrupted (increased roughness) and several aggregates accumulated on the bilayer within 1–3 h (Fig. 2d). The observed morphological changes associated with the bilayer were similar to those observed at later time points when exposed to htt exon1(35Q) or htt exon1(46Q). After ~12 h (Fig. 2d), nearly the entire bilayer displayed a roughened morphology, indicative of disrupted bilayer structural integrity. Interestingly, fibrils of these constructs were not observed, despite literature reports indicating that these constructs form fibrils without the presence of a lipid membrane at similar concentration and timescales [11]. This observation suggests that the bilayer either promotes the formation of aggregates

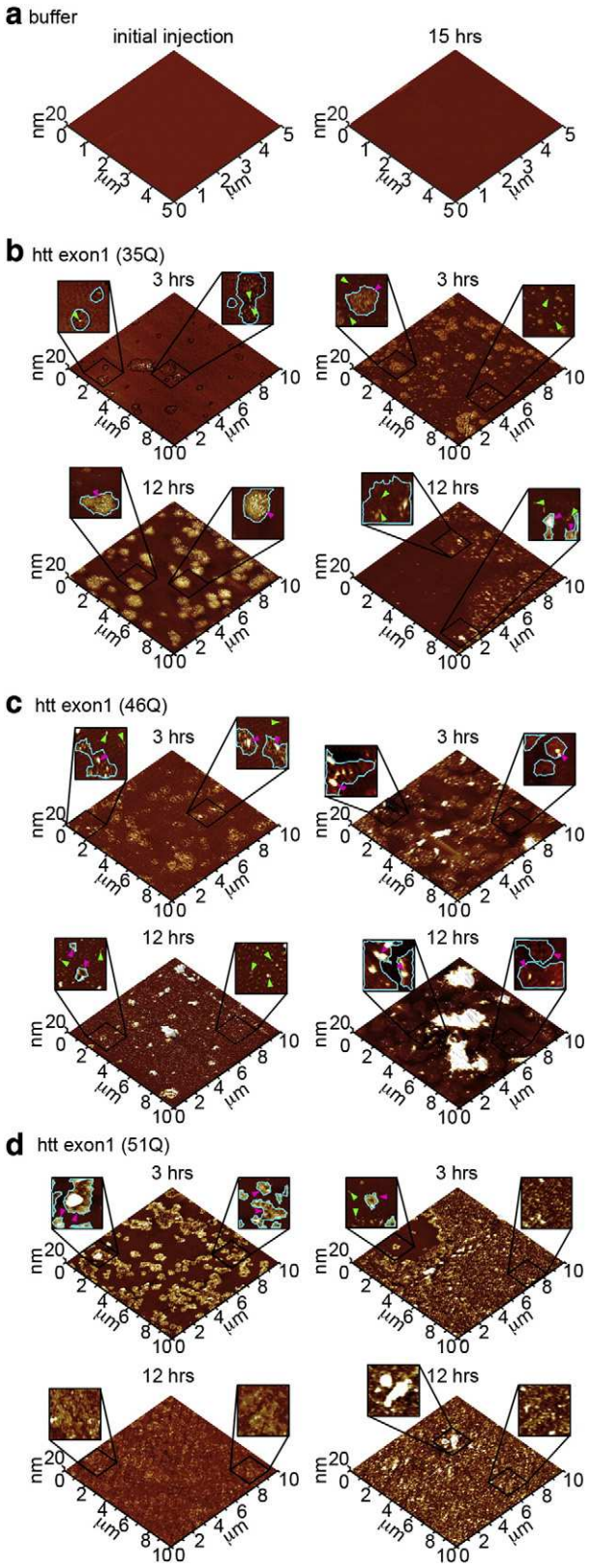

Fig. 2. Htt exon1 binds to and disrupts the morphology of TBLE bilayers. TBLE bilayers were exposed to (a) buffer vehicle, fresh preparation of (b) htt exon1(35Q), (c) htt exon1(46Q), or (d) htt exon1 (51Q). Images taken at different time points are presented as 3D reconstructions (10 × 10 μm) with indicated zoomed in 2 × 2 μm areas presented in 2D. In the 2D representations, green arrows indicate oligomers, pink arrows indicate amorphous aggregates, and blue outlines areas of increased surface roughness.

off pathway to fibrils or that aggregate intermediates are stabilized by interaction with lipid membranes.

In an effort to quantify the extent of interaction between the TBLE bilayer and different htt exon1 constructs, analysis of the AFM images was performed. First, the (root mean squared) RMS roughness of the perturbed regions of the bilayer was measured (Fig. 3a). A freshly formed, defect-free bilayer had a RMS surface roughness of 0.25 ± 0.01 nm measured over a total of 40 μm^2. To prevent error associated with the size of the regions of disrupted bilayer structure, RMS roughness measurements of areas that had been destabilized by htt exon1 constructs were restricted only to portions of the images containing disruption, and thus excluding regions of the bilayer not altered by the presence of htt exon1 from the analysis. RMS roughness measurements are also highly dependent on the coverage of htt exon1 aggregates present on the surface; therefore, aggregate structures were filtered out of the analysis.

Within the first four hours of exposure to the different htt exon1 constructs, regions of the bilayer that were significantly rougher ($p < 0.01$) than unperturbed bilayer were observed for all three htt exon1 proteins, and the measured roughness increased with increasing polyQ length. That is, htt exon1(35Q) caused the smallest increase in surface roughness (0.59 ± 0.07 nm), htt exon1(46Q) induced a significantly larger increase in surface roughness (1.48 ± 0.12 nm), and htt exon1(51Q) resulted in the largest increase in surface roughness (2.58 ± 0.17 nm). After 12 h of exposure, the bilayer surface roughness associated with exposure to all three htt exon1 constructs increased. While the roughness associated with exposure to htt exon1(35Q) (1.48 ± 0.19 nm) was still significantly smaller compared to the other two constructs, the increased roughness associated with htt exon1(46Q) (5.80 ± 0.51 nm) and htt exon1(51Q) (6.79 ± 0.67 nm) was similar, indicating that there may be an upper limit to the amount of increased roughness associated with exposure to htt exon1 proteins and that reaching this state occurs more rapidly with longer polyQ length.

As the previous analysis was confined just to regions of the bilayer that exhibited increased roughness, we next wanted to determine the extent of bilayer disruption as a function of polyQ length. To accomplish these, we determined the percentage of the surface that displayed any increased roughness (Fig. 3b). At early (1–4 h after) exposure and later (12–16 h after) exposure there was a tendency for longer polyQ lengths to be associated with a larger extent of bilayer disruption. At the early time point, htt exon1(51Q) resulted in a significantly ($p < 0.01$) larger area of bilayer disruption compared to the other two constructs. At 12–16 h (Fig. 3b), bilayers exposed to htt exon1 (46Q) had a significantly ($p < 0.05$) larger extent of disruption compared to bilayers exposed to htt exon1 (35Q), and htt exon1(51Q) caused a larger extent of bilayer disruption ($p < 0.01$) than htt exon1 (46Q). Collectively, the two analyses demonstrate a rough dependence on polyQ length on the disruption of bilayer integrity.

3.2. Nt17 facilitates the interaction of htt exon1 with lipid bilayers

To determine if Nt17 facilitates the interaction between htt exon1 and lipid bilayers, we compared the lipid interaction of myc-htt exon1(53Q), which contains a ten amino acid long myc-tag as well as 11 more vector derived amino acids directly adjacent to htt exon1's N-terminus, with that of htt exon1 (51Q), which only has three additional vector derived residues on the N-terminus. These two constructs have similar length polyQ domains and have been shown to form fibrils at a similar rate in the absence of a surface [34]. We hypothesized that the addition of the additional 21 amino acids, including the myc-tag, to the N-terminus of htt exon1 would inhibit the ability of the protein to bind the lipid bilayer. Myc-htt exon1 (53Q) was prepared in the same manner as the htt exon1(51Q) construct; however, PreScission Protease was used to cleave the GST moiety in htt proteins with the myc-tag. A potential complication in interpreting these studies is that

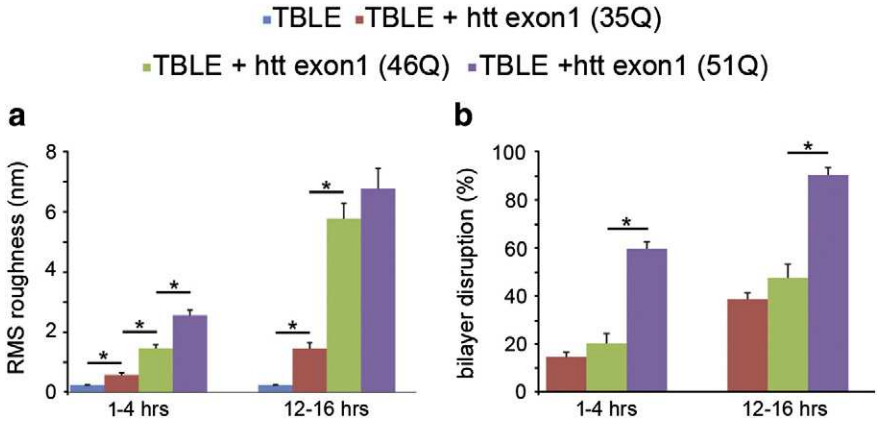

Fig. 3. Htt exon1 disrupts TBLE bilayers in a polyQ length dependent manner. (a) Quantification of root mean squared (RMS) surface roughness and (b) percent bilayer disrupted by exposure to htt exon1(35Q), htt exon1(46Q), or htt exon1(51Q) at 1–4 h and 12–16 h as assessed by AFM images. * indicates $p < 0.01$.

the PreScission Protease is more efficient in cleaving GST compared to Factor Xa (Fig. 1c).

Upon injection of 20 μM myc-htt exon1(53Q) to the lipid bilayer, discrete, oligomeric and some large amorphous aggregates appeared on the bilayer within 1–4 h (Fig. 4). These aggregates were stable and appeared to be immobile, as they appeared unaltered in subsequent AFM images. Regions of increased surface roughness were also observed. After ~12 h (Fig. 4) of exposure to myc-htt exon1(53Q), the extent of bilayer disruption and the size and number of aggregates increased. While similar aggregate morphologies compared to those observed for htt exon1(51Q) were observed, highly-branched fibrillar structures of myc-htt exon1(53Q) also formed on the surface. These fibrillar structures still were morphologically different than fibrils observed for the same constructs without the presence of a lipid surface [34].

We then used image analysis to quantitatively compare the impact of bilayer exposure to htt exon1(51Q) and myc-htt exon1(53Q) (Fig. 5). While both constructs increased the surface roughness of the bilayer, the addition of the myc tag significantly reduced the magnitude of the surface roughness at both early (1.47 ± 0.07 nm) and later (4.10 ± 0.51 nm) time points. Furthermore, the area of bilayer affected (roughened) by the exposure to htt exon1 was also significantly impeded by the addition of the myc-tag, indicating that blocking or altering the N-terminus of htt exon1 reduces the efficiency

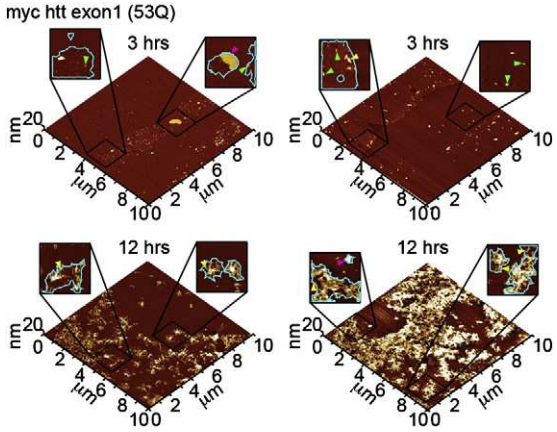

Fig. 4. Freshly prepared TBLE bilayers were exposed to 20 μM myc-htt exon1 (53Q). AFM images of myc-htt exon1(53Q) aggregates on TBLE bilayers at 3 and 12 h. Images are presented as 3D reconstructions (10 × 10 μm) with indicated zoomed in 2 × 2 μm areas presented in 2D. In the 2D representations, green arrows indicate oligomers, pink arrows indicate amorphous aggregates, and blue outlines areas of increased surface roughness.

of its interaction with lipid membranes. This reduced ability of myc-htt exon1 (53Q) to deposit on and disrupt the membrane was observed despite the higher efficiency of the PreScission Protease, which would result in a larger amount of free peptide.

3.3. Pre-aggregation inhibits the interaction of htt exon1 with lipid bilayers

In order to determine if larger htt aggregates directly interact with lipid bilayers, TBLE bilayers were exposed to pre-aggregated (8 h of incubation) myc-htt exon1 (53Q). At this time point, myc-htt exon1(53Q) was predominately aggregated into a variety of oligomers and large fibrils [11,34]. Upon injection of the 20 μM pre-aggregated myc-htt exon1(53Q) into the fluid cell, little to no interaction with the bilayer was observed as determined by the appearance of aggregates or increase surface roughness (Fig. 6). The bilayers remained stable and unaltered as assessed by AFM for over 24 h.

3.4. Htt exon1 induces mechanical changes in lipid bilayers

To determine if exposure to htt exon1 altered bilayer mechanics, SPAM was used to directly assess bilayer rigidity and adhesive properties by reconstructing the time-resolved tip/sample tapping forces associated with imaging the surface with tapping mode AFM in solution. While the total force per tapping event remains constant at any given set of AFM imaging parameters, specific features of the time-resolved tapping force are sensitive mechanical properties of the surfaces [39,40]. Specifically, the maximum tapping force (F_{max}), defined as the peak or largest positive force experienced between the tip and surface during one tapping event, increases with larger values of surface elastic modulus with a power law dependence.

[40,41]. Additionally, the minimum tapping force (F_{min}), defined as the peak or largest negative force experienced between the tip and surface during one tapping event, is directly proportional to the adhesive energy between the tip and surface. As a result, monitoring F_{max} and F_{min} while obtaining an AFM image allows for mapping the relative rigidity and adhesive properties of the bilayer, which can be directly associated with topographical features of the surface.

Force maps, as well as histograms of the forces associated with every tapping event, were constructed of TBLE bilayers exposed to htt exon1(51Q) (Fig. 7). The F_{max} associated with regions of the bilayer perturbed (increased surface roughness) by exposure to htt exon1(51Q) was significantly reduced in magnitude, indicating that a softening or decrease in the elastic modulus of these regions compared to unperturbed regions of the bilayer (Fig. 7a). The magnitude of F_{min} associated with the perturbed regions of the bilayer also decreased compared to unperturbed regions of the bilayer (Fig. 7b),

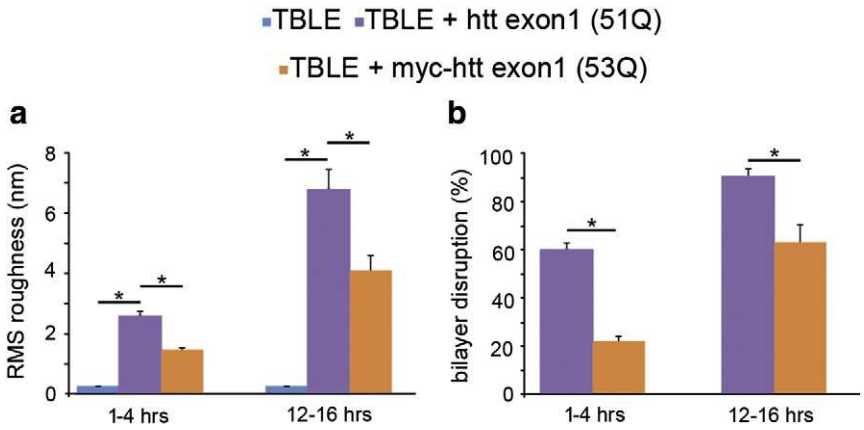

Fig. 5. Addition of an N-terminal myc tag as well as other vector derived residues inhibits the ability of htt exon1 to disrupt TBLE bilayers. (a) Quantification of root mean squared (RMS) surface roughness and (b) percent bilayer disrupted by exposure to htt exon1(51Q) or myc-htt exon1(53Q) at 1–4 h and 12–16 h as assessed by AFM images. * indicates $p < 0.01$.

which correlates to a reduced adhesive interaction between the AFM tip and bilayer in the regions with increased surface roughness. These observed changes in rigidity and adhesion are consistent with a decreased order of lipid component packing required to compensate for protein insertion/binding, thus resulting in a rougher bilayer that is more easily compressed by the AFM tip.

4. Discussion

In this study, we determined how the interaction of htt exon1 with TBLE bilayers is polyQ length dependent, facilitated by the availability of the Nt17 domain of htt, and aggregation state. We also evaluated the mechanical impact on lipid bilayers of exposure to htt exon1. The culmination of these findings emphasizes the importance of polyQ length and Nt17 on aggregation rates and resulting aggregate morphologies of mutant htt exon1 in the presence of lipid membranes. Our results support the notion that monomeric htt and/or pre-fibrillar aggregates may play a causative role in HD pathogenesis by directly binding subcellular surfaces and directly altering membrane integrity. While we used TBLE bilayers as model membranes for these studies, it is unlikely that this membrane would perfectly mimic the composition of lipids in actual cellular and subcellular surfaces as membranes in the brain are heterogeneous depending on cell type, brain regions, and intracellular compartments. As a result, further studies are justified to elucidate the interaction of htt with different model membranes and cellular surfaces.

Several aggregation pathways have been proposed for the formation of fibrils of polyQ-containing proteins in free solution. Commonly, two aggregation schemes are proposed. The first requires the rearrangement of a monomer to a thermodynamically unfavorable conformation that directly nucleates fibrillization [12]. The second scenario proceeds via the formation of soluble oligomeric intermediates that undergo a structural re-arrangement leading to fibril formation [11,42,43]. Some studies suggest that these two schemes are not mutually exclusive [11]. In general, it appears that pure polyQ peptide, i.e., no flanking sequences, prefers to aggregate from monomers directly to fibrils [44–46]; although, some studies have questioned this interpretation [47,48]. It has been suggested that the addition of flanking sequences, in particular Nt17, can shift the aggregation

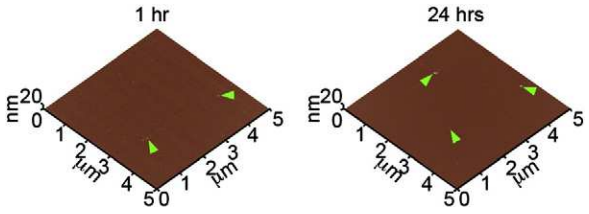

Fig. 6. Freshly prepared TBLE bilayers were exposed to 20 μM myc-htt exon1(53Q). AFM images of myc-htt exon1(53Q) aggregates on TBLE bilayers at 1 and 24 h. Green arrows indicate oligomeric aggregates formed on the bilayer surface.

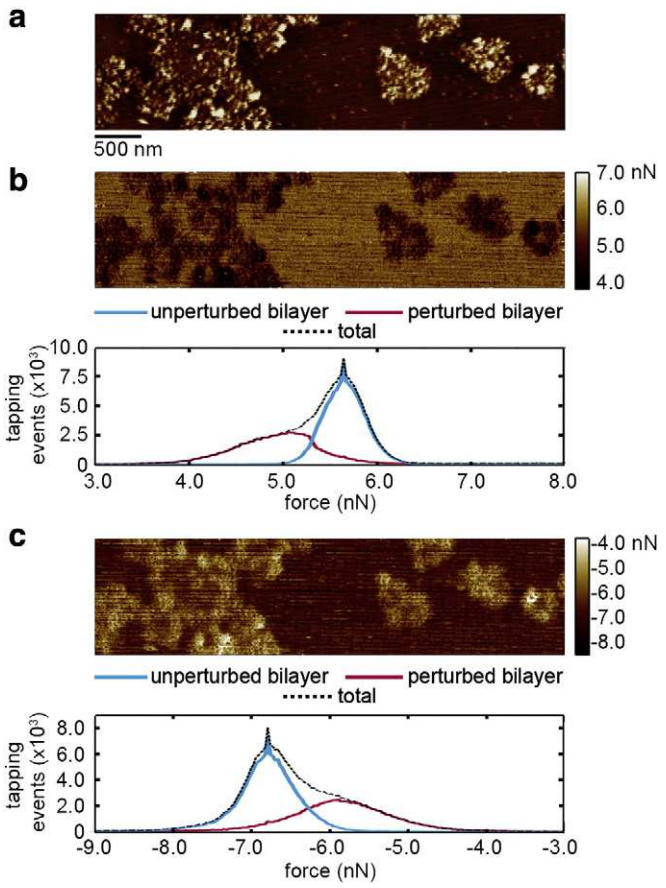

Fig. 7. Exposing TBLE bilayers to htt exon1(51Q) resulted in local regions of reduced Young's modulus and adhesion to the AFM tip. (a) Topography image of TBLE bilayer exposed to htt exon1(51Q). SPAM images and histograms of (b) the maximum tapping force (F_{max}) and (c) the minimum tapping force (F_{min}) that correspond to the topography image are also presented. The reduced F_{max} associated with the regions of the bilayer with perturbed morphology indicates a lower elastic modulus. The reduced F_{min} associated with the regions of the bilayer with perturbed morphology indicates reduced adhesive interaction between the bilayer and AFM tip.

process toward the pathway that includes oligomeric intermediates [14,42,43]. However, these aggregation schemes can be further complicated by environmental factors such as surfaces [49], and our study indicates that lipid membranes can further modulate the aggregation process, favoring the formation of amorphous accumulations of htt exon1 and small oligomers.

Our studies indicate that htt exon1/lipid interaction is highly dependent on polyQ length. While previous studies indicate that htt exon1 and synthetic polyQ peptides aggregate into numerous different species [11,42,43], including fibrils and oligomers, our results demonstrate that amorphous accumulations of htt exon1 are the predominant aggregate species formed at the liquid/lipid interface. However, some oligomers were bound to the bilayer surface, and fibril-like morphologies were observed when a myc-tag was added to the N-terminus of htt exon1.

While htt fragments with expanded polyQ domains are predominately located in microscopic inclusion bodies in the cytoplasm and nucleus in HD brains [3], htt has been shown to be directly associated with a variety of membranous surfaces such as mitochondria, endoplasmic reticulum, tubulovesicles, endosomes, lysosomes and synaptic vesicles [4,50]. The environments associated with these subcellular membrane surfaces could profoundly affect the aggregation of htt with expanded polyQ domains. For example, lipid membranes could act as nucleation sites by promoting/stabilizing specific aggregate prone conformation, orienting monomers to faciliate aggregation, or by creating local areas of high htt concentration. The potential role of such membranes in htt aggregation is supported by observations in cellular models that membraneous structures are directly incorporated onto the surfaces of htt inclusion bodies [51] and that htt aggregates accumulate lipids in transgenic mice [52,53]. N-terminal fragments of htt are associated with membrane when isolated from HD brains [54]. Studies with large unimolecular vesicles demonstrated that association of htt with lipid surfaces was highly dependent on phospholipid content [29].

In our study, the ability of htt exon1 to directly interact with TBLE bilayers is directly correlated to length of the polyQ domain. It has been well established in synthetic polyQ peptides that the longer the polyQ stretch the faster the rate of aggregation in free solution [43–46,55,56]. This aggregation rate dependence on polyQ length has been experimentally verified in htt exon1 constructs [11], and these observations are consistent with a causative role for htt aggregation in HD pathogenesis. In light of these studies, it would be reasonable to interpret the observed polyQ-length dependence on htt interaction arising from the increased aggregation rate with longer polyQ domains. However, the aforementioned aggregation studies were not performed in the presence of a lipid membrane, and the aggregate morphologies were distinctly different compared to the aggregates observed on TBLE bilayer here, suggesting there may be other mitigating factors involved. For example, a recent study using a variety of synthetic polyQ peptides suggested that there was a polyQ length dependence on the formation and stability of the amphipathic α-helix associated with Nt17 [42]. While this Nt17 α-helix has been linked to the formation of oligomers [42,43], it also targets membranes [24,52,57,58]. The stabilization of this Nt17 α-helix based on polyQ length may be playing an indirect role critical to the association of htt exon1 with lipid membranes, reinforcing the polyQ-length dependence on htt/lipid interactions.

The notion that Nt17 facilitates the interaction between htt and lipid membranes is further supported by our observations that an N-terminal myc-tag can inhibit the ability of htt exon1 to directly interact with TBLE bilayers. This suggests that Nt17's amphipathic α-helix is either sterically blocked or structurally altered by the myc-tag, reducing the efficiency by which it binds bilayers. Notably, there was a distinct morphological difference between aggregates of myc-htt exon1(53Q) on the bilayer compared to aggregates comprised of htt exon1(51Q). As a result, there appears to be a myc-tag facilitated mechanism to form highly-branched, fibril-like aggregates on the bilayer surface. Such observations are interesting in light of studies that indicate that exogenous tags to htt constructs alter toxicity in yeast models of HD [59]. Recent studies have even noted post-translational modifications to Nt17 alter aggregation state [60] and subcellular localization [61] of htt, and these modifications could further modify the interaction of htt with lipid bilayers.

The Nt17 domain promotes the formation of oligomeric intermediates on pathway to fibril formation [42,43], whereas, pure polyQ peptides prefer to form fibrils directly from monomer precursors [62]. The importance of Nt17 in promoting oligomer formation has also been demonstrated in htt exon1, as the addition of the same N-terminal myc-tag used in this study reduced oligomer formation without any effect on fibrillization [34]. While targeting the Nt17 has been demonstrated to alter htt aggregation [60], the efficiency of such a strategy may be reduced due the presence of lipid surfaces. Such a scenario was observed experimentally when (−)-epigallocatechin gallate (EGCG) was less effective at inhibiting aggregation of human islet amyloid polypeptide at a phospholipid interface [63].

Our mechanical analysis of TBLE bilayers demonstrates that exposure to htt exon1 locally alters the compressibility of the bilayer and reduces the adhesive interaction between the AFM tip and bilayer. These mechanical alterations to the lipid bilayer induced by htt exon1 could underlie membrane dysfunction previously observed in animal models [3,26]. The mechanical changes could be due to a local disordering of bilayer lipid components to accommodate the binding and aggregation of htt exon1 within the bilayer. Such a scenario is consistent with the increased surface roughness associated with these mechanically altered domains. Disordering of the lipid bilayer induced by expanded htt exon1 could jeopardize membrane integrity and lead directly to membrane dysfunction. Lipid/htt interactions are also relevant in the trafficking of htt within the cell [64–66]. Previous studies have speculated that lipid mechanics are directly correlated with dysfunction and disease [67–69] as elasticity and adhesion are hypothesized to influence cellular and sub-cellular stabilities. Understanding how alterations in lipid stability and mechanics relate to polyQ length and the N-terminal α-helix could aid in identifying the precise mechanism that mediates pathogenesis in HD.

Acknowledgements

This work was supported by the Brodie Discovery and Innovation Fund and the National Science Foundation (NSF#1054211). CSU was supported by the West Virginia University Summer Undergraduate Research Experience Program. KMH was supported by the WVnano REU Program (DMR-1004431; PI, Michelle Richards-Babb; Co-PI, David Lederman).

References

[1] The Huntington's Disease Collaborative Research Group, A novel gene containing a trinucleotide repeat that is expanded and unstable on Huntington's disease chromosomes cell, 72 (1993) 971–983.
[2] B. Wilburn, D.D. Rudnicki, J. Zhao, T.M. Weitz, Y. Cheng, X. Gu, E. Greiner, C.S. Park, N. Wang, B.L. Sopher, A.R. La Spada, A. Osmand, R.L. Margolis, Y.E. Sun, X.W. Yang, An antisense CAG repeat transcript at JPH3 locus mediates expanded polyglutamine protein toxicity in Huntington's disease-like 2 mice, Neuron 70 (2011) 427–440.
[3] S.W. Davies, M. Turmaine, B.A. Cozens, M. DiFiglia, A.H. Sharp, C.A. Ross, E. Scherzinger, E.E. Wanker, L. Mangiarini, G.P. Bates, Formation of neuronal intranuclear inclusions underlies the neurological dysfunction in mice transgenic for the HD mutation, Cell 90 (1997) 537–548.
[4] M. DiFiglia, E. Sapp, K.O. Chase, S.W. Davies, G.P. Bates, J.P. Vonsattel, N. Aronin, Aggregation of huntingtin in neuronal intranuclear inclusions and dystrophic neurites in brain, Science 277 (1997) 1990–1993.
[5] L. Mangiarini, K. Sathasivam, M. Seller, B. Cozens, A. Harper, C. Hetherington, M. Lawton, Y. Trottier, H. Lehrach, S.W. Davies, G.P. Bates, Exon 1 of the HD gene with an expanded CAG repeat is sufficient to cause a progressive neurological phenotype in transgenic mice, Cell 87 (1996) 493–506.
[6] R.G. Snell, J.C. Macmillan, J.P. Cheadle, I. Fenton, L.P. Lazarou, P. Davies, M.E. Macdonald, J.F. Gusella, P.S. Harper, D.J. Shaw, Relationship between trinucleotide

repeat expansion and phenotypic variation in Huntington's-disease, Nat. Genet. 4 (1993) 393–397.
[7] J.B. Penney, J.P. Vonsattel, M.E. MacDonald, J.F. Gusella, R.H. Myers, CAG repeat number governs the development rate of pathology in Huntington's disease, Ann. Neurol. 41 (1997) 689–692.
[8] A.J. Tobin, E.R. Signer, Huntington's disease: the challenge for cell biologists, Trends Cell Biol. 10 (2000) 531–536.
[9] E. Scherzinger, R. Lurz, M. Turmaine, L. Mangiarini, B. Hollenbach, R. Hasenbank, G.P. Bates, S.W. Davies, H. Lehrach, E.E. Wanker, Huntingtin-encoded polyglutamine expansions form amyloid-like protein aggregates in vitro and in vivo, Cell 90 (1997) 549–558.
[10] E. Scherzinger, A. Sittler, K. Schweiger, V. Heiser, R. Lurz, R. Hasenbank, G.P. Bates, H. Lehrach, E.E. Wanker, Self-assembly of polyglutamine-containing huntingtin fragments into amyloid-like fibrils: implications for Huntington's disease pathology, Proc. Natl. Acad. Sci. U. S. A. 96 (1999) 4604–4609.
[11] J. Legleiter, E. Mitchell, G.P. Lotz, E. Sapp, C. Ng, M. DiFiglia, L.M. Thompson, P.J. Muchowski, Mutant huntingtin fragments from oligomers in a polyglutamine length-dependent manner in vitro and in vivo, J. Biol. Chem. 285 (2010) 14777–14790.
[12] S.M. Chen, V. Berthelier, J.B. Hamilton, B. O'Nuallain, R. Wetzel, Amyloid-like features of polyglutamine aggregates and their assembly kinetics, Biochemistry 41 (2002) 7391–7399.
[13] A. Bhattacharyya, A.K. Thakur, V.M. Chellgren, G. Thiagarajan, A.D. Williams, B.W. Chellgren, T.P. Creamer, R. Wetzel, Oligoproline effects on polyglutamine conformation and aggregation, J. Mol. Biol. 355 (2006) 524–535.
[14] V.N. Sivanandam, M. Jayaraman, C.L. Hoop, R. Kodali, R. Wetzel, P.C.A. van der Wel, The aggregation-enhancing huntingtin N-terminus is helical in amyloid fibrils, J. Am. Chem. Soc. 133 (2011) 4558–4566.
[15] A. Lunkes, J.L. Mandel, A cellular model that recapitulates major pathogenic steps of Huntington's disease, Hum. Mol. Genet. 7 (1998) 1355–1361.
[16] F. Saudou, S. Finkbeiner, D. Devys, M.E. Greenberg, Huntingtin acts in the nucleus to induce apoptosis but death does not correlate with the formation of intranuclear inclusions, Cell 95 (1998) 55–66.
[17] A.S. Hackam, R. Singaraja, C.L. Wellington, M. Metzler, K. McCutcheon, T.Q. Zhang, M. Kalchman, M.R. Hayden, The influence of huntingtin protein size on nuclear localization and cellular toxicity, J. Cell Biol. 141 (1998) 1097–1105.
[18] M. Arrasate, S. Mitra, E.S. Schweitzer, M.R. Segal, S. Finkbeiner, Inclusion body formation reduces levels of mutant huntingtin and the risk of neuronal death, Nature 431 (2004) 805–810.
[19] P.J. Muchowski, Protein misfolding, amyloid formation, and neurodegeneration: a critical role for molecular chaperones? Neuron 35 (2002) 9–12.
[20] M.W. Kim, Y. Chelliah, S.W. Kim, Z. Otwinowski, I. Bezprozvanny, Secondary structure of huntingtin amino-terminal region, Structure 17 (2009) 1205–1212.
[21] J. Legleiter, G.P. Lotz, J. Miller, J. Ko, C. Ng, G.L. Williams, S. Finkbeiner, P.H. Patterson, P.J. Muchowski, Monoclonal antibodies recognize distinct conformational epitopes formed by polyglutamine in a mutant huntingtin fragment, J. Biol. Chem. 284 (2009) 21647–21658.
[22] J.D. Godin, K. Colombo, M. Molina-Calavita, G. Keryer, D. Zala, B.C. Charrin, P. Dietrich, M.-L. Volvert, F. Guillemot, I. Dragatsis, Y. Bellaiche, F. Saudou, L. Nguyen, S. Humbert, Huntingtin is required for mitotic spindle orientation and mammalian neurogenesis, Neuron 67 (2010) 392–406.
[23] L.R. Gauthier, B.C. Charrin, M. Borrell-Pages, J.P. Dompierre, H. Rangone, F.P. Cordelieres, J. De Mey, M.E. MacDonald, V. Lessmann, S. Humbert, F. Saudou, Huntingtin controls neurotrophic support and survival of neurons by enhancing BDNF vesicular transport along microtubules, Cell 118 (2004) 127–138.
[24] R.S. Atwal, J. Xia, D. Pinchev, J. Taylor, R.M. Epand, R. Truant, Huntingtin has a membrane association signal that can modulate huntingtin aggregation, nuclear entry and toxicity, Hum. Mol. Genet. 16 (2007) 2600–2615.
[25] R.S. Atwal, R. Truant, A stress sensitive ER membrane-association domain in huntingtin protein defines a potential role for huntingtin in the regulation of autophagy, Autophagy 4 (2008) 91–93.
[26] M. Difiglia, E. Sapp, K. Chase, C. Schwarz, A. Meloni, C. Young, E. Martin, J.P. Vonsattel, R. Carraway, S.A. Reeves, F.M. Boyce, N. Aronin, Huntingtin is a cytoplasmic protein associated with vesicles in human and rat-brain neurons, Neuron 14 (1995) 1075–1081.
[27] K.B. Kegel, E. Sapp, J. Alexander, A. Valencia, P. Reeves, X. Li, N. Masso, L. Sobin, N. Aronin, M. DiFiglia, Polyglutamine expansion in huntingtin alters its interaction with phospholipids, J. Neurochem. 110 (2009) 1585–1597.
[28] K.B. Kegel, E. Sapp, J. Yoder, B. Cuiffo, L. Sobin, Y.J. Kim, Z.H. Qin, M.R. Hayden, N. Aronin, D.L. Scott, F. Isenberg, W.H. Goldmann, M. DiFiglia, Huntingtin associates with acidic phospholipids at the plasma membrane, J. Biol. Chem. 280 (2005) 36464–36473.
[29] K.B. Kegel, V. Schewkunow, E. Sapp, N. Masso, E.E. Wanker, M. DiFiglia, W.H. Goldmann, Polyglutamine expansion in huntingtin increases its insertion into lipid bilayers, Biochem. Biophys. Res. Commun. 387 (2009) 472–475.
[30] A. Di Pardo, V. Maglione, M. Alpaugh, M. Horkey, R.S. Atwal, J. Sassone, A. Ciammola, J.S. Steffan, K. Fouad, R. Truant, S. Sipione, Ganglioside GM1 induces phosphorylation of mutant huntingtin and restores normal motor behavior in Huntington disease mice, Proc. Natl. Acad. Sci. U. S. A. 109 (2012) 3528–3533.
[31] P.J. Muchowski, G. Schaffar, A. Sittler, E.E. Wanker, M.K. Hayer-Hartl, F.U. Hartl, Hsp70 and Hsp40 chaperones can inhibit self-assembly of polyglutamine proteins into amyloid-like fibrils, Proc. Natl. Acad. Sci. U. S. A. 97 (2000) 7841–7846.
[32] J. Legleiter, M. Park, B. Cusick, T. Kowalewski, Scanning probe acceleration microscopy (SPAM) in fluids: mapping mechanical properties of surfaces at the nanoscale, Proc. Natl. Acad. Sci. U. S. A. 103 (2006) 4813–4818.
[33] J.L. Hutter, J. Bechhoefer, Calibration of atomic-force microscope tips, Rev. Sci. Instrum. 64 (1993) 1868–1873.
[34] K.A. Burke, J. Godbey, J. Legleiter, Assessing mutant huntingtin fragment and polyglutamine aggregation by atomic force microscopy, Methods 53 (2011) 275–284.
[35] J. Legleiter, R.B. DeMattos, D.M. Holtzman, T. Kowalewski, In situ AFM studies of astrocyte-secreted apolipoprotein E- and J-containing lipoproteins, J. Coll. Interf. Sci. 278 (2004) 96–106.
[36] J.T. Groves, N. Ulman, S.G. Boxer, Micropatterning fluid lipid bilayers on solid supports, Science 275 (1997) 651–653.
[37] J. Jass, T. Tjarnhage, G. Puu, From liposomes to supported, planar bilayer structures on hydrophilic and hydrophobic surfaces: an atomic force microscopy study, Biophys. J. 79 (2000) 3153–3163.
[38] C.M. Yip, E.A. Elton, A.A. Darabie, M.R. Morrison, J. McLaurin, Cholesterol, a modulator of membrane-associated A beta-fibrillogenesis and neurotoxicity, J. Mol. Biol. 311 (2001) 723–734.
[39] B. Kumar, P.M. Pfifer, A. Giovengo, J. Legleiter, The effect of set point ratio and surface Young's modulus on maximum tapping forces in fluid tapping mode atomic force microscopy. (vol 107, 044508, 2010) J. Appl. Phys. 107 (2010).
[40] N. Shamitko-Klingensmith, K.M. Molchanoff, K.A. Burke, G.J. Magnone, J. Legleiter, Mapping the mechanical properties of cholesterol-containing supported lipid bilayers with nanoscale spatial resolution, Langmuir 28 (2012) 13411–13422.
[41] K.A. Burke, E.A. Yates, J. Legleiter, Amyloid-forming proteins alter the local mechanical properties of lipid membranes, Biochemistry 52 (2013) 808–817.
[42] M. Jayaraman, R. Kodali, B. Sahoo, A.K. Thakur, A. Mayasundari, R. Mishra, C.B. Peterson, R. Wetzel, Slow amyloid nucleation via alpha-helix-rich oligomeric intermediates in short polyglutamine-containing huntingtin fragments, J. Mol. Biol. 415 (2012) 881–899.
[43] A.K. Thakur, M. Jayaraman, R. Mishra, M. Thakur, V.M. Chellgren, I.-J.L. Byeon, D.H. Anjum, R. Kodali, T.P. Creamer, J.F. Conway, A.M. Gronenborn, R. Wetzel, Polyglutamine disruption of the huntingtin exon 1 N terminus triggers a complex aggregation mechanism, Nat. Struct. Mol. Biol. 16 (2009) 380–389.
[44] K. Kar, M. Jayaraman, B. Sahoo, R. Kodali, R. Wetzel, Critical nucleus size for disease-related polyglutamine aggregation is repeat-length dependent, Nat. Struct. Mol. Biol. 18 (2011) 328.
[45] N. Slepko, A.M. Bhattacharyya, G.R. Jackson, J.S. Steffan, J.L. Marsh, L.M. Thompson, R. Wetzel, Normal-repeat-length polyglutamine peptides accelerate aggregation nucleation and cytotoxicity of expanded polyglutamine proteins, Proc. Natl. Acad. Sci. U. S. A. 103 (2006) 14367–14372.
[46] A.M. Bhattacharyya, A.K. Thakur, R. Wetzel, Polyglutamine aggregation nucleation: thermodynamics of a highly unfavorable protein folding reaction, Proc. Natl. Acad. Sci. U. S. A. 102 (2005) 15400–15405.
[47] R.H. Walters, R.M. Murphy, Aggregation kinetics of interrupted polyglutamine peptides, J. Mol. Biol. 412 (2011) 505–519.
[48] R.H. Walters, R.M. Murphy, Examining polyglutamine peptide length: a connection between collapsed conformations and increased aggregation, J. Mol. Biol. 393 (2009) 978–992.
[49] K.A. Burke, E.A. Yates, J. Legleiter, Biophysical insights into how surfaces, including lipid membranes, modulate protein aggregation related to neurodegeneration, Front. Neuroanat. 4 (2013) 17.
[50] C.A. Gutekunst, S.H. Li, H. Yi, J.S. Mulroy, S. Kuemmerle, R. Jones, D. Rye, R.J. Ferrante, S.M. Hersch, X.J. Li, Nuclear and neuropil aggregates in Huntington's disease: relationship to neuropathology, J. Neurosci. 19 (1999) 2522–2534.
[51] K.B. Kegel, M. Kim, E. Sapp, C. McIntyre, J.G. Castano, N. Aronin, M. DiFiglia, Huntingtin expression stimulates endosomal–lysosomal activity, endosome tubulation, and autophagy, J. Neurosci. 20 (2000) 7268–7278.
[52] J. Suopanki, C. Gotz, G. Lutsch, J. Schiller, P. Harjes, A. Herrmann, E.E. Wanker, Interaction of huntingtin fragments with brain membranes — clues to early dysfunction in Huntington's disease, J. Neurochem. 96 (2006) 870–884.
[53] A. Valencia, P.B. Reeves, E. Sapp, X.Y. Li, J. Alexander, K.B. Kegel, K. Chase, N. Aronin, M. DiFiglia, Mutant huntingtin and glycogen synthase kinase 3-beta accumulate in neuronal lipid rafts of a presymptomatic knock-in mouse model of Huntington's disease, J. Neurosci. Res. 88 (2010) 179–190.
[54] Y.J. Kim, Y. Yi, E. Sapp, Y.M. Wang, B. Cuiffo, K.B. Kegel, Z.H. Qin, N. Aronin, M. DiFiglia, Caspase 3-cleaved N-terminal fragments of wild-type and mutant huntingtin are present in normal and Huntington's disease brains, associate with membranes, and undergo calpain-dependent proteolysis, Proc. Natl. Acad. Sci. U. S. A. 98 (2001) 12784–12789.
[55] S.M. Chen, F.A. Ferrone, R. Wetzel, Huntington's disease age-of-onset linked to polyglutamine aggregation nucleation, Proc. Natl. Acad. Sci. U. S. A. 99 (2002) 11884–11889.
[56] M.J. Bennett, K.E. Huey-Tubman, A.B. Herr, A.P. West, S.A. Ross, P.J. Bjorkman, A linear lattice model for polyglutamine in CAG-expansion diseases, Proc. Natl. Acad. Sci. U. S. A. 99 (2002) 11634–11639.
[57] M. Michalek, E.S. Salnikov, S. Werten, B. Bechinger, Membrane interactions of the amphipathic amino terminus of huntingtin, Biochemistry 52 (2013) 847–858.
[58] K.A. Burke, K.J. Kauffman, C.S. Umbaugh, S.L. Frey, J. Legleiter, The interaction of polyglutamine peptides with lipid membranes is regulated by flanking sequences associated with huntingtin, J. Biol. Chem. 288 (2013) 14993–15005.
[59] M.L. Duennwald, S. Jagadish, P.J. Muchowski, S. Lindquist, Flanking sequences profoundly alter polyglutamine toxicity in yeast, Proc. Natl. Acad. Sci. U. S. A. 103 (2006) 11045–11050.
[60] R. Mishra, M. Jayaraman, B.P. Roland, E. Landrum, T. Fullam, R. Kodali, A.K. Thakur, I. Arduini, R. Wetzel, Inhibiting the nucleation of amyloid structure in a huntingtin fragment by targeting alpha-helix-rich oligomeric intermediates, J. Mol. Biol. 415 (2012) 900–917.
[61] R.S. Atwal, C.R. Desmond, N. Caron, T. Maiuri, J. Xia, S. Sipione, R. Truant, Kinase inhibitors modulate huntingtin cell localization and toxicity, Nat. Chem. Biol. 7 (2011) 453–460.

[62] A.K. Thakur, R. Wetzel, Mutational analysis of the structural organization of polyglutamine aggregates, Proc. Natl. Acad. Sci. U. S. A. 99 (2002) 17014–17019.
[63] M.F.M. Engel, C.C. VandenAkker, M. Schleeger, K.P. Velikov, G.H. Koenderink, M. Bonn, The polyphenol EGCG inhibits amyloid formation less efficiently at phospholipid interfaces than in bulk solution, J. Am. Chem. Soc. 134 (2012) 14781–14788.
[64] J.P. Caviston, E.L.F. Holzbaur, Huntingtin as an essential integrator of intracellular vesicular trafficking, Trends Cell Biol. 19 (2009) 147–155.
[65] O. Cremona, G. Di Paolo, M.R. Wenk, A. Luthi, W.T. Kim, K. Takei, L. Daniell, Y. Nemoto, S.B. Shears, R.A. Flavell, D.A. McCormick, P. De Camilli, Essential role of phosphoinositide metabolism in synaptic vesicle recycling, Cell 99 (1999) 179–188.
[66] A.L. Orr, S. Li, C.-E. Wang, H. Li, J. Wang, J. Rong, X. Xu, P.G. Mastroberardino, J.T. Greenamyre, X.-J. Li, N-terminal mutant huntingtin associates with mitochondria and impairs mitochondrial trafficking, J. Neurosci. 28 (2008) 2783–2792.
[67] H.D. Hong, L.K. Tamm, Elastic coupling of integral membrane protein stability to lipid bilayer forces, Proc. Natl. Acad. Sci. U. S. A. 101 (2004) 4065–4070.
[68] V. Vogel, M. Sheetz, Local force and geometry sensing regulate cell functions, Nat. Rev. Mol. Cell Biol. 7 (2006) 265–275.
[69] P.A. Janmey, D.A. Weitz, Dealing with mechanics: mechanisms of force transduction in cells, Trends Biochem. Sci. 29 (2004) 364–370.